ISSN 1064-2269, Journal of Communications Technology and Electronics, 2008, Vol. 53, No. 8, pp. 934–940. © Pleiades Publishing, Inc., 2008.
Original Russian Text © A.K. Kalabukhov, M.L. Chukharkin, A.A. Deleniv, D. Winkler, I.A. Volkov, O.V. Snigirev, 2008, published in Radiotekhnika i Elektronika, 2008, Vol. 53, No. 8, pp. 987–993.

PHYSICAL PROCESSES IN ELECTRON DEVICES

Analysis of the Possibility to Amplify an RF Signal with a Superconducting Quantum Interference Filter

A. K. Kalabukhov, M. L. Chukharkin, A. A. Deleniv, D. Winkler, I. A. Volkov, and O. V. Snigirev

Received May 15, 2007

Abstract—A laboratory prototype RF amplifier for the frequency range 1–10 GHz is designed, created, and tested. The device is based on high-temperature superconducting quantum interference filters (SQUIFs) and the technology of bicrystalline substrates. The main characteristics of the prototype SQUIF amplifier are numerically simulated and measured.

PACS numbers: 85.25.Dq, 84.30.Le

DOI: 10.1134/S1064226908080111

INTRODUCTION

Cryogenic RF amplifiers based on low-temperature superconducting (LTSC) quantum interferometers (SQUIDs) exhibit the record-low noise temperature $T_n = 50 \pm 10$ mK at a frequency of 0.5 GHz and a temperature of 0.1 K [1]. This noise temperature is approximately 40 times lower than the noise temperature that can be realized at such frequencies via the use of low-temperature semiconductor amplifiers with relatively high carrier mobility [2, 3]. The typical gains of LTSC SQUIDs are about 20 and 10–12 dB at frequencies below 1 GHz and from 1 to 4 GHz, respectively [4, 5]. Note that the power consumption of a SQUID amplifier is lower than the power consumption of its semiconductor analog by several orders of magnitude. The main disadvantage of SQUID amplifiers is a narrow dynamic range, which corresponds to a small linear section on the sine-shape voltage–field characteristic (VFC). Negative feedback, which is widely employed at low (up to 10 MHz) frequencies can hardly be used at high frequencies [6]. The VFC range and, hence, the dynamic range of an amplifier are determined only by characteristic voltage V_{ch} of Josephson junctions.

In addition, the characteristic voltage determines the maximum gain and the working frequency of a SQUID. From the radiophysical point of view, a SQUID can be classified as a particular case of a parametric amplifier in which the pump frequency is the Josephson oscillation frequency: $F_J = 2\pi V_{ch}/\Phi_0$, where $\Phi_0 = 2 \times 10^{-15}$ Wb is the flux quantum. The maximum gain of a SQUID is determined by the ratio of the Josephson frequency to signal frequency F_s [7]:

$$G \le F_J/F_s = 2\pi V_{ch}/\Phi_0 F_s. \quad (1)$$

This expression makes it possible to interpret the observed decrease in the gain of LTSC SQUIDs with an increase in the signal frequency from 1 to 8 GHz. (The measured gain decreases from 20 to 5 dB [8].)

The characteristic voltage of junctions is determined only by the superconducting material and the SQUID working temperature. For three-layer ($Nb/AlO_x/Nb$) Josephson junctions used in LTSC SQUIDs, this voltage is no greater than 100–200 μV. For high-temperature superconducting (HTSC) SQUIDs (at $T = 4$ K), the characteristic voltage can be at least an order of magnitude higher than that of LTSC SQUIDs. Therefore, it is of interest to realize an RF amplifier based on an HTSC SQUID in which the VFC range and the signal conversion steepness V_Φ ($V_\Phi = \Delta V/\Delta\Phi \approx V_{ch}/\Phi_0$) can be greater by an order of magnitude [9]. The dynamic range and V_Φ can be additionally increased with a superconducting quantum interference filter (SQUIF) [10, 11].

The simplest SQUIF is a 1D array of series- or parallel-connected SQUIDs. If the areas of the quantization loops of the interferometers do not satisfy a general regularity (are randomly distributed), the SQUIF VFC is a single peak at zero magnetic field. In the series-connected SQUIF, the peak height increases with the number of interferometers [12]. This circumstance is an evident advantage of a SQUIF microwave amplifier in comparison with a conventional SQUID: A significantly greater VFC range determines the maximum gain and dynamic range. Obviously, the SQUIF disadvantage of a SQUIF lies in the fact that the linear dimension of the array is substantially greater than the dimension of a single SQUID. This circumstance impedes SQUIF matching of the SQUIF with an external signal source at a high frequency.

The purpose of this study is to analyze the possibility of realizing a laboratory prototype RF amplifier for the frequency range 1–10 GHz based on a series-connected HTSC SQUIF.

At the first stage, we develop the general configuration and design of a series-connected HTSC SQUIF on a bicrystalline substrate. Then, we match the series-connected interferometer array with a 50-Ω signal source in the frequency range 0.1–10.0 GHz. We numerically simulate a SQUIF-based microwave amplifier, present the main stages of the device construction, and discuss the characteristics of the SQUIF amplifier that are obtained from dc and microwave measurements.

1. AMPLIFIER TOPOLOGY

The main elements of a SQUIF-based amplifier are located in the layers of a thin-film integrated structure. The SQUIF structure with necessary contact pads is located in the lower HTSC (YBCO) layer. The antenna that transfers the signal to the SQUIF is located in the upper normal-metal (Au) layer that is separated from the HTSC film by a dielectric (SiO_2) layer.

We design the structure with allowance for the fact that, at a frequency of 5 GHz, the electromagnetic wave length is 6 cm and, hence, the electromagnetic wave length in SiO_2 ($\varepsilon \approx 3.8$) is $\lambda \approx 3$ cm. Thus, the amplifier structure can be treated as a lumped structure if the length of the SQUID array is no greater than $\lambda/8 \approx 3.5$ mm.

The SQUIF VFC exhibits a single developed peak when the number of SQUIDs is $N \geq 30$ [12]. An increase in number N of SQUIDs leads to an increase in the conversion steepness; the dynamic range; and, naturally, the length of the structure at a fixed minimum technological increment (3 μm in the case under study). In the first experiments, we choose $N = 50$, which represents a reasonable compromise between the technological and electrodynamic requirements.

In addition, an increase in N results in an increase in dynamic resistance R_d of the SQUIF whose impedance must be close to a load impedance of 50 Ω. For the typical HTSC devices, for which R_d of a single SQUID is 1–2 Ω, the resistance of N series-connected interferometers ranges from 50 to 100 Ω. Thus, we employ the series-connected variant of the SQUIF, although, in comparison with the parallel variant, it is more sensitive to the spread of the parameters of the Josephson junctions [13].

Figure 1 demonstrates the mask pattern of a series-connected SQUIF that consists of 50 interferometers with receiving-circuit areas that are randomly distributed in the range 40–400 μm^2. Each interferometer circuit is a slit with a fixed thickness of 4 μm in the HTSC film. The width of the Josephson junctions is 3 μm. For the measurements of the interferometer characteristics, the SQUIF structure contains additional contact pads and the corresponding connections to seven partial SQUIF interferometers.

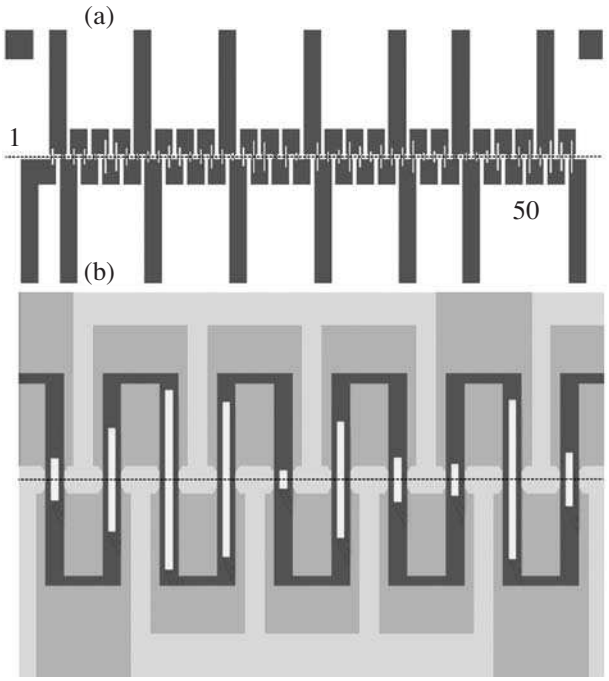

Fig. 1. (a) Mask pattern of the SQUIF structure and (b) a fragment of the SQUIF array with the position of the slot line. The dashed line shows the position of the bicrystalline junction.

For applying an external HF signal, we design a slot line that is formed in a layer of normal metal (a gold film with a thickness of 200 nm that is produced via magnetron sputtering). The slot line is insulated from the HTSC film with a 400-nm-thick SiO_2 layer that is likewise produced via magnetron sputtering. In the simplest case, the configuration of the slot line with a thickness of 10 μm is a meander that is located above the SQUIF structure and envelopes each interferometer, thus providing for the maximum magnetic-flux coupling (Fig. 1b). The line is closed at the end of the SQUIF structure, so that the slot line can be considered a closed coil at low frequencies. The total length of the slot line is 2.5 mm.

2. SIMULATION OF THE PROCESSES

In the framework of the classical approach, when $M_i \leq L$, power gain G of a single interferometer is given by [14]

$$G \approx (M_i V_\Phi)^2 \frac{1}{R_d R_i} = \left(\frac{M_i}{L}\right)^2 \frac{R_d}{R_i} \propto n^2 L, \qquad (2)$$

where M_i is the mutual inductance between the interferometer circuit and the input coil, L is the inductance of the interferometer loop, R_d is the SQUID dynamic resistance, and R_i is the input-circuit dissipation that can be determined from the Q factor of the input circuit.

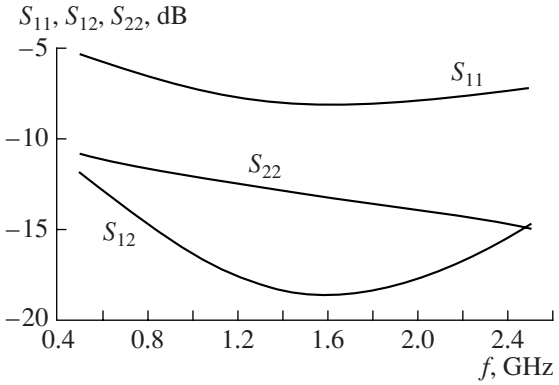

Fig. 2. The S parameters calculated in the range 1–8 GHz for the input antenna shown in Fig. 1b.

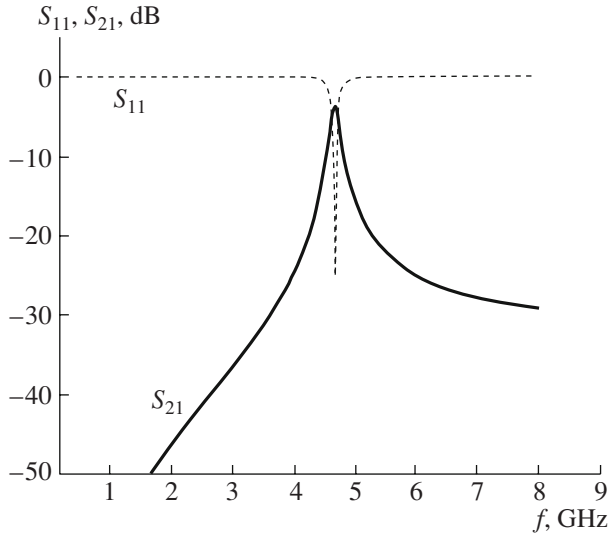

Fig. 3. The S parameters calculated for a more complicated circuit of the input antenna.

For the N-interferometer SQUIF, effective mutual inductance M_{eff} is on the order of NM_{i}.

A relatively high gain G can be realized at high circular currents at the signal frequency in the SQUID circuit. Such gains provide for the parametric conversion in the SQUID junctions and, hence, the signal amplification. Note the important role of the input dynamic impedances of single SQUIDs in the calculation of the mutual inductance of the slot line and the SQUIF. The input impedances are known for frequencies of about 1 kHz and 100 MHz [15, 16]. For the frequency range under study, the impedance data are unavailable. In the first approximation, we can assume that, for the circular current at a high signal frequency comparable with the characteristic Josephson frequency, the impedance of each partial interferometer is close to $2R$, where R is the normal resistance of the Josephson junction [17].

To simulate the processes in the SQUIF amplifier, we employ the Agilent RF Design Environment 2003C (RFDE Momentum) software [18]. In the calculations, the input of the slot line is connected to a signal generator with an impedance of 50 Ω, while the SQUIF is connected to a 50-Ω load. The value of R ranges from 1 to 10 Ω.

Figure 2 shows the S parameters calculated for the input circuit shown in Fig. 1b in the range 1–8 GHz.

Figure 3a presents the S parameters calculated for a more complicated input circuit in the range 1–8 GHz. The reflection of the input signal is insignificant (S_{11} = –15 dB); hence, the input power is absorbed in the slot line, which is inductively coupled to the SQUIF interferometer array.

To estimate the power gain of the SQUIF amplifier, we must determine mutual inductance M_{i} of the slot line and a single interferometer (see expression (2)). For this purpose, in the simulation procedure, the Josephson junctions in one of the interferometers are changed by a current meter and the values of ring current I_{r} are determined upon the slot line excitation at the signal power P = 0 dBm (1 mW).

In this case, the external flux in the interferometer loop is $M_{\text{i}} \times I_e$, where I_e is the current that flows in the matched 50-Ω slot line:

$$I_e = (8P/\text{Re}Z)^{1/2} = 13 \text{ mA}. \quad (3)$$

If normal inductance β_L is greater than unity, the external flux is almost completely compensated by the self-induction flux of the interferometer LI_{r}. This flux is produced by ring current I_{r}. Using the standard formula from [19] to estimate the geometric inductance of the interferometer with internal contour dimensions of 4 × 50 μm, we can directly estimate mutual inductance M_{i}:

$$M_{\text{i}} = L\Delta I_{\text{r}}/\Delta I_e \approx 5 \text{ pH}. \quad (4)$$

Using expressions (2) and (4), we can find the maximum power gain. For the above method of signal application by means of a slot line, a power gain of greater than unity can be realized if the minimum value of the SQUIF transfer function is no less than 1 mV per flux quantum.

3. CREATION OF A PROTOTYPE SQUIF AMPLIFIER

We create both three samples that contain test structures of SQUIFs in the absence of the input slot line and an array of 50 identical SQUIDs with the area corresponding to the maximum area of the SQUIF interferometer. All of the devices are created on YSZ (Y–ZrO_2) bicrystalline substrates with off-orientation angles of 24° (12°/12°). To create the structures, we employ optical photolithography and dry etching in an argon-ion beam. Laser sputtering is applied to deposit

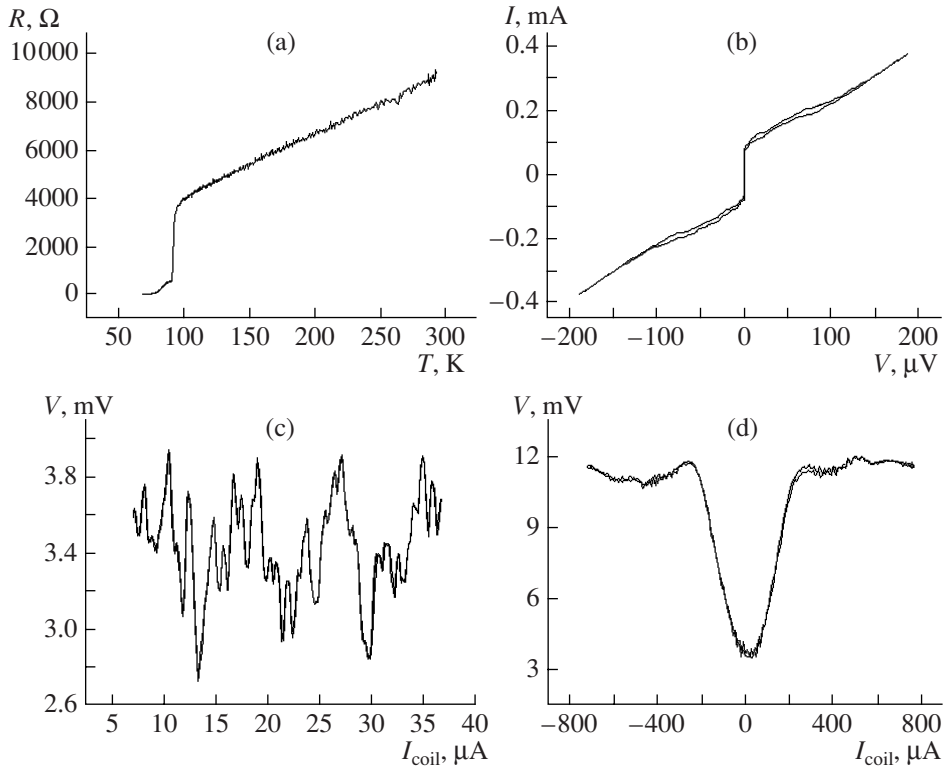

Fig. 4. (a) Plot of resistance vs. SQUIF temperature, (b) *I–V* characteristic, and (c, d) VFCs in two ranges of the magnetic field.

$Y_1Ba_2Cu_3O_7$ (YBCO) films with a thickness of 200–250 nm. First, we deposit the buffer (CeO_2) layer at the substrate temperature $T_{sub} = 790°C$ and an oxygen pressure of 0.2 mbar to provide the high-quality growth of an HTSC film near the bicrystalline interface. Then, YBCO films are sputtered at the temperature $T_{sub} = 780°C$ and an oxygen pressure of 0.7 mbar in the absence of vacuum interruption.

For both the CeO_2 buffer layer and the YBCO film, the deposition processes were preliminarily optimized on YSZ single-crystal substrates to reach relatively high critical parameters of the films, in particular, low roughness of the surface, a high critical temperature, and a high critical current density.

The X-ray analysis of the crystalline structure of the film indicates the absence of the *a–b* oriented phases. The rotation of the CeO_2 film relative to the substrate (45°) corresponds to the optimal growth of the CeO_2 film with the minimum deviation of the lattice parameters.

An atomic force microscope (AFM) is used to test the film surface. The typical roughness of the films (R_a) is no greater than 5 nm, which is sufficient to prevent the contact of the HTSC film with the upper gold layer via the insulator. The critical temperatures of the YBCO films are 87–89 K at $\Delta T < 1$ K. The critical current density of the film is $J_{cr} = 2 \times 10^6$ A/cm^2.

4. DC MEASUREMENTS

The technological spread of the parameters of Josephson junctions can lead to the incoherent interaction of the interferometers in the SQUIF structure. This circumstance can lead to the absence of a single peak on the VFC. To test the created SQUIFs, we measure the low-frequency response of the samples with respect to the magnetic field in the temperature range 4–77 K. First, for all of the structures, we determine the critical and normal parameters T_{cr}, I_{cr}, and R_n of the SQUIF (Fig. 4) and seven single SQUIDs. The response to the external magnetic field is measured with an external bias coil that has a conversion coefficient of 22 μT/mA. The measurements are performed with Permalloy shields, which allow the Earth's magnetic field and external interference to be substantially suppressed. The results show the presence of several sharp peaks (Fig. 4c) rather than a single SQUIF peak.

To interpret this result, we measure the spread of critical currents and normal resistance for the accessible single SQUIDs in two SQUIFs. The ratio of the square deviation of the measured critical currents to the mean value is close to 30%.

Note the three most probable causes of such a significant spread of the critical currents of the junctions. The first is the technological spread of the junction widths at the production stage. Thus, the junctions exhibit different effective areas, which can be estimated

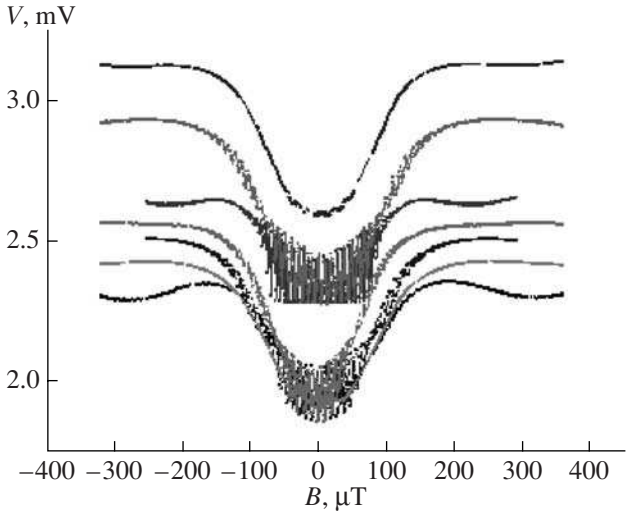

Fig. 5. VFCs of partial SQUIDs measured at a temperature of 40 K.

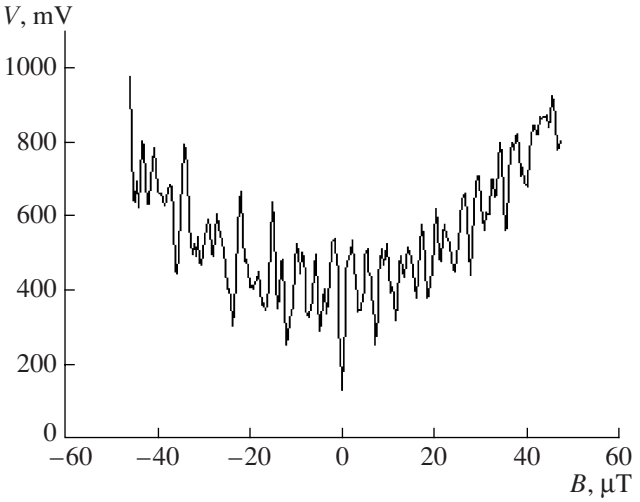

Fig. 6. VFC of the SQUIF created on an $SrTiO_3$ bicrystalline substrate.

from the position of the first minimum on the diffraction dependence of the Josephson junction critical current on the magnetic field [20]. The test measurements on seven partial interferometers yield a relatively small (about 8%) spread of the junction widths.

Another possible cause of the spread of the critical currents is the heterogeneity of the transport properties of the barrier along the bicrystalline interface. It is known that the transport properties of the grain-boundary junctions (in particular, bicrystalline junctions) are well described with the Glazman–Matveev model for tunneling through localized states [21]. In this case, there is a fundamental relationship between the characteristic voltage $V_{ch} = I_{cr}R_n$ and critical current density J_{cr} $V_{ch} \sim (J_{cr})^p$, where $p \approx 0.5$. In the case under study, we do not observe such a root dependence of the characteristic voltage of the junctions on the critical current density. This circumstance indicates that the spread of the critical currents of the junctions is not determined by the heterogeneity of the critical current density of the junctions along the bicrystalline interface.

The last cause is the spread of the HTSC-film thickness in the junction region at the bicrystalline interface. This interface always contains a region with defect crystalline properties, where the normal epitaxial growth of a film is impossible. Therefore, a layer of the HTSC film with the perturbed structure that does not exhibit superconducting properties grows in the interface region at the initial stage. Because of the further sputtering, this layer appears covered by a high-quality HTSC film. The thickness of the perturbed layer is primarily determined by the quality of the bicrystalline junction.

To verify this assumption, we create a structure on a high-quality $SrTiO_3$ bicrystalline substrate. The resulting SQUIF exhibits a significantly narrower spread of the junction parameters in the array. (The spread of the critical currents is 20%.) Figure 6 demonstrates the VFC of the above structure with a singe characteristic peak of the SQUIF.

5. MICROWAVE MEASUREMENTS

To measure the characteristics of the SQUIF amplifier in the microwave range, we additionally form the total structures of the input coil as a slot line on two samples created on YSZ substrates. The absence of the main single peak on the SQUIFs in the vicinity of the zero field does not impede the amplifier testing, and the maximum response (of about 1 mV) is substantially greater than the VFC amplitude of known similar LTSC devices. (The details of the measurement system can be found in our previous work [3] devoted to the study of the microwave characteristics of SQUID amplifiers.) The sample, a thermometer, and a coil that generates the external magnetic field (used for the SQUIF bias with respect to the magnetic flux) are located on a Teflon circuit board with a thickness of 0.8 mm. The board is placed in a metal box with two subminiature *A*-type connectors (SMA) used to set and measure the microwave signal. A dc bias is set with a *T* insulator, and the output signal is measured with a cooled low-noise amplifier. (The noise temperature is 6 K at an amplifier temperature of 20 K.) Prior to the SQUIF mounting, we calibrate the input and output circuits. The *S* parameters are measured with a Rohde & Schwarz RS-20 vector network analyzer.

Figure 7 demonstrates the measured frequency dependence of the SQUIF-amplifier output signal. The maximum difference between the output power of the SQUIF amplifier at the optimal bias current and flux

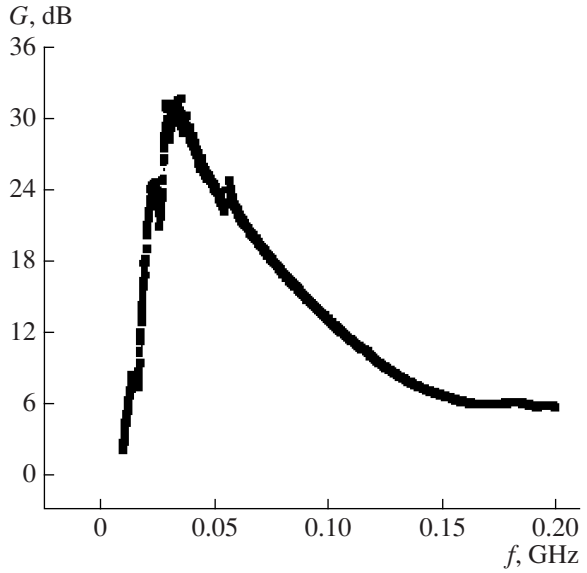

Fig. 7. Plot of maximum difference G between the output powers of the SQUIF amplifier vs. frequency. The result is obtained at the optimal bias current and flux and at the zero bias current.

and the output power at the zero bias current is 30 dB. This difference determines the maximum reachable SQUIF power gain in the absence of loss in the input circuit. To estimate the real gain, we measure the transmission coefficient of the total circuit at a low temperature in the absence of a SQUIF. The true power gain appears to be no greater than 5 dB. In addition, it is seen from Fig. 7 that the maximum amplified signal is observed at a frequency of 100 MHz, which is significantly lower than the calculated frequency for the input circuit (5 GHz).

The results directly indicate the occurrence of loss in the input coil of the SQUID. This condition leads to both a decrease in the gain and a significant shift of the working frequency. One of the causes of the loss is the application of a thin (in comparison with the skin-layer depth) gold film (200 nm) for the creation of the slot line. The insufficient magnetic-flux coupling between the input coil and partial interferometers may be a more significant factor leading to a low gain. The above problems will be studied in detail in future investigations.

CONCLUSIONS

The main purpose of this study has been to create a high-temperature SQUIF and to analyze the possibility of its application as an RF amplifier. In the framework of this problem, we have numerically simulated the processes in various configurations of input antennas. Data on the creation of HTSC interference filters on YSZ bicrystalline substrates have been collected. The main characteristics of samples have been measured. Prototype SQUIF amplifiers have been created on single chips. For the first time, we have measured the high-frequency response of a SQUIF-amplifier. The maximum reachable gain is 30 dB, and the real gain is 5 dB at a frequency of 100 MHz owing to the loss in the input circuit.

For the practical application of the SQUIF amplifiers, we need to solve the problem related to the spread of parameters of Josephson junctions and the transfer of an RF signal from the antenna to the distributed SQUIF structure in the absence of additional loss.

The first problem is a fundamental problem for all series-connected HTSC SQUIFs. It can be partially solved owing to the better quality of bicrystalline substrates. However, the partial solution can impede the practical application of SQUIFs as microwave amplifiers. A better approach involves the improvement of the parameters of classical HTSC quantum interferometers and the realization of coupling with the input antenna. The last problem (which is significantly simplified in the case of a single interferometer) can be solved by means of a comprehensive study that includes the calculation of the input circuit with allowance for the dynamic parameters of the SQUID and the improvement of the SQUID creation technology.

The accumulated data on the creation of HTSC SQUIFs and the integrated structures of input antennas of the slot-line type can be used in the further development of a cryogenic low-noise microwave amplifier.

ACKNOWLEDGMENTS

This study was supported by the US Civilian Research and Development Foundation (CRDF) (grant RUE1-1610-MO-05) and the Russian Federal Agency for Science and Innovation (state contract no. 02.514.11.4012).

REFERENCES

1. M. Mück, J. B. Kycia, and J. Clarke, Appl. Phys. Lett. **78**, 967 (2001).
2. R. F. Bradley, Nucl. Phys. A. **72** (1), 137 (1999).
3. I. Lopes-Fernandez, J. D. G. Puyol, O. J. Homan, and A. B. Cancio, Microwave Guid. Wave Lett. **9** (10), 413 (1999).
4. G. V. Prokopenko, S. V. Shitov, I. L. Lapitskaya, et al., IEEE Trans. Appl. Supercond. **13**, 1042 (2003).
5. A. S. Kalabukhov, M. A. Tarasov, E. A. Stepantsov, et al., Physica C **368** (1–4), 171 (2002).
6. M. Mück, Physica A **368** (1–4), 141 (2002).
7. G. V. Prokopenko, S. V. Shitov, I. V. Borisenko, and J. Mygand, IEEE Trans. Appl. Supercond. **13**, 1046 (2003).
8. M. Mück, C. Welzel, and J. Clarke, Appl. Phys. Lett. **82**, 3266 (2003).
9. E. Stepantsov, M. Tarasov, A. Kalabukhov, et al., J. Appl. Phys. **96**, 3357 (2004).
10. J. Oppenlaender, C. Haeussler, A. Friesch, et al., IEEE Trans. Appl. Supercond. **15**, 936 (2005).

11. P. Caputo, J. Oppenländer, C. Häussler, et al., Appl. Phys. Lett. **85**, 1389 (2004).

12. J. Oppenlaender, C. Haeussler, T. Träeuble, and N. Schopohl, Physica C **368** (1–4), 119 (2002).

13. V. Schultze, R. Ijsselsteijn, R. Boucher, et al., Supercond. Sci. Technol. **16**, 1356 (2003).

14. C. Hilbert and J. Clarke, J. Low Temp. Phys. **61** (3–4), 263 (1985).

15. C. Hilbert and J. Clarke, J. Low Temp. Phys. **61** (3–4), 237 (1985).

16. P. Falferi, R. Mezzena, S. Vitale, and M. Cherdonio, Appl. Phys. Lett. **71**, 956 (1997).

17. K. K. Likharev and B. T. Ul'rikh, *Systems with Josephson Contacts. Principles of Theory* (Mosk. Gos. Univ., Moscow, 1978), p. 65 [in Russian].

18. http://eesof.tm.agilent.com/products/rfde2003c-momentum.html.

19. M. B. Ketchen, W. J. Gallagher, and A. W. Kleisasser, in *SQUID'85: Superconducting Quantum Interference Devices and their Applications*, Ed. by H.-D. Hahlbohm and H. Lubbig (Walter de Gruyter & Co, Berlin, 1985), p. 856.

20. P. A. Rosental, M. R. Beasley, K. Char, et al., Appl. Phys. Lett. **59**, 3482 (1991).

21. R. Gross, P. Chaudhari, M. Kawasaki, and A. Gupta, Phys. Rev. B **42**, 10735 (1998).